The Effect of Vegetation Enhancement on Particulate Pollution Reduction: CFD Simulations in an Urban Park

Hongqiao Qin, Bo Hong *, Runsheng Jiang, Shanshan Yan and Yunhan Zhou

College of Landscape Architecture & Arts, Northwest A&F University, Yangling 712100, China;
hongqiao@nwafu.edu.cn (H.Q.); jrs_96@nwafu.edu.cn (R.J.); Yanshanshan@nwafu.edu.cn (S.Y.);
zhouyh@nwafu.edu.cn (Y.Z.)
* Correspondence: hongbo@nwsuaf.edu.cn; Tel.: +86-029-8708-0269

check for
updates

Abstract: Vegetation in parks is regarded as a valuable way to reduce particulate pollution in urban environments but there is little quantitative information on its effectiveness. The aim of this study was to conduct on-site measurements and computational fluid dynamic (CFD) simulations to determine the aerodynamic and deposition effects of vegetation enhancement on particulate matter (PM) dispersions in an urban park in Xi'an, China. Initially, the airflow characteristics and deposition effects of vegetation were predicted and compared with measured air velocities and particulate pollution data to validate the numerical modeling. Then, associated coverage ratios and supplementary green areas (tree coverage ratio, crown volume coverage (*CVC*), and roof greening) were added to numerical simulations. After a series of numerical simulations and comparisons, results indicated that: (1) Numerical models with simplified vegetation method could reproduce the distribution of particulate matter concentrations in the real park environment; (2) with a tree coverage ratio >37.8% (or $CVC > 1.8$ m^3/m^2), the pedestrian-level PM$_{2.5}$ could meet the World Health Organization's air quality guidelines (IT-1) standards in the park; (3) roof greening on leeward buildings produced greater PM removal effects compared with windward buildings; and (4) the most economical and reasonable tree coverage ratio and *CVC* to reduce atmospheric PM in urban parks should be 30% and 1.8 m^3/m^2, respectively. These results are useful guidelines for urban planners towards a sustainable design of vegetation in urban parks.

Keywords: urban park; particulate matter; computational fluid dynamics (CFD); tree coverage ratio; crown volume coverage (*CVC*)

1. Introduction

Atmospheric aerosol particulate matter (PM) refers to a variety of suspended solid and liquid pollutants. Inhalable particles, with an aerodynamics diameter smaller than 10 μm and 2.5 μm (PM$_{10}$ and PM$_{2.5}$), not only reduce human working efficiency and happiness [1–3], but inhalable particles can cause a range of respiratory and cardiovascular diseases and increase the incidence of malignant tumors [4–7]. Studies in Europe, the United States, and many Asian cities have shown that increased, and longer exposure to, particulate concentrations increase the risk of morbidity and mortality [8–10]. As a result, air pollution caused by PM has attracted much public and scientific attention.

Urban green infrastructure can relieve heat island effects and play an important role in improving the urban air quality [11–14]. Trees in green infrastructure can effectively reduce PM in urban environments [15–19]. Tree species, canopy size, canopy porosity, leaf area density (LAD), and tree arrangements around buildings can all affect the particulate diffusion [20,21]. Recently, numerous

studies have discussed the deposition velocity or particulate capture efficiency of various tree species through wind tunnel experiments or field studies [22–27]. Methods include mass subtraction [28,29], membrane filters [30–34], and elution weighing coupled with particle size analysis by electron microscopy [35–40], along with other direct measuring methods with aerosol instruments [41–43]. These studies largely analyze the deposition rate of PM on leaves [44,45], as well as changes in retention duration of different PM sizes on leaf surfaces [46]. Numerical simulations generally quantitatively analyze aerodynamic and deposition effects of vegetation on PM dispersion in built environments [47–56], or investigate the influences of outdoor PM diffusion into indoor spaces by constructing three dimensional models [57,58]. Additionally, related research has been conducted on the deposition effects of green roofs on particulate matters [59]. Vegetation on roofs could reduce more pollution rather than crops grown near roads [60].

As a component of urban green infrastructure, parks play an important role in reducing PM in urban air [61,62]. Research demonstrates that the average pollutant concentration in parks is lower closer to the center of treed areas [63]. Yin et al. (2011) analyzed pollutant concentration changes in a Shanghai park and found that the crown volume coverage (*CVC*) increased from 0 to 2 m^3/m^2, the TSP, SO_2, and NO_2 removal rates increased by 30%, 15%, and 10%, respectively [61]. Research elsewhere indicates that tree coverage ratio in urban parks is a major factor affecting PM retention [64].

Abundant field tests and simulation studies demonstrate that trees can effectively reduce atmospheric PM. However, studies have principally focused on effects of vegetation structure or tree species [24,27,29]. Due to instrumental constraint, results from field experimental studies can record parameters in only a limited time and space without fully reflecting the dynamic meteorological and environmental conditions, and using more stations would have been costly. Therefore, they do not provide generalize guidance on urban park design. With the aid of simulation based on computational fluid dynamics (CFD), the simplified models simulating the particulate matter dispersion in a block or urban scale has been significantly advanced [65]. Numerical simulations can solve the problem of environmental control, save time and labor, and are not limited by time and space. Using controlled variables in a street or urban scale simulation, the effect of trees on atmospheric particles dispersion can be directly calculated using the Reynolds-averaged Navier–Stokes (RANS) model combined with the generalized drift flux model [20,58,63].

In this study, we used CFD based models, including a standard *k-ε* model based on the RANS approach and a revised generalized drift flux model, to quantitatively investigate: (1) the accuracy of numerical models using simplified vegetation method; and (2) effects of changing supplementary green areas and associated coverage ratios (tree coverage ratio, *CVC*, and roof greening) on $PM_{2.5}$ and PM_{10} reduction. Our results could provide optimal methods and quantitative indices for tree design in urban parks for the goal of environmental improvement.

2. Methods

2.1. Study Site

The study park is located in Xi'an, China (34°15′56.2″ N, 108°4′21.5″ E). The park's footprint is 13.3 ha, and the building area is approximately 16,000 m^2. The park is a natural garden style with four main buildings (Bldg.1—China agricultural history museum, Bldg.2—Botanical museum, Bldg.3—Animal museum, and Bldg.4—Insect museum). The landscape elements in the park are as follows: buildings (accounting for 10 percent of the total area), plants (accounting for 75 percent of the total area), paving and square (accounting for 10 percent of the total area), water-filled pool (accounting for 5 percent of the total area). The north and east sides of the park are adjacent to a main thoroughfare. The west and south sides are adjacent to a university campus (Figure 1).
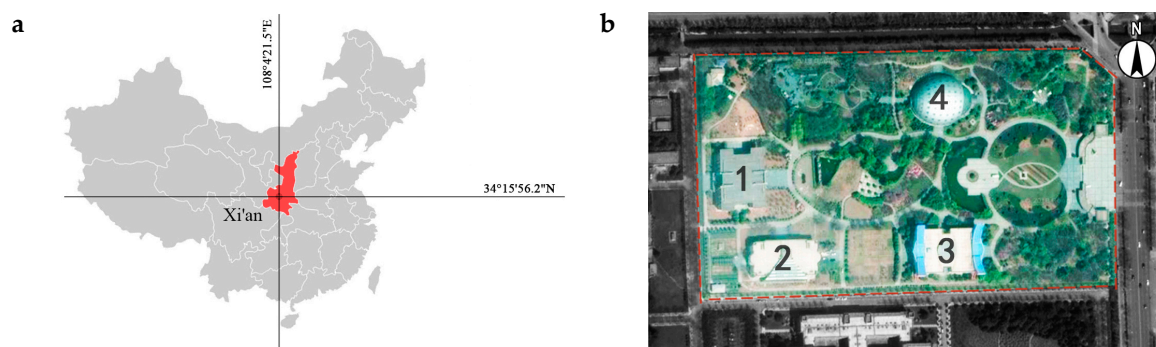
Figure 1. Location of the study site (**a**) and a Google map (**b**).

2.2. On-Site Measurement

Twelve monitored points were fixed in the park to record wind speed and direction (Kestrel 5500 wind speed meter, Nielsen-Kellerman Inc., Boothwyn, PA, USA) as well as PM concentrations (Aerocet 531S, Met One Inc., Grants Pass, OR, USA) at 1.5 m height. Monitored point *A* is fixed on the roof of the Bldg.3 to record incoming wind speed, wind direction and PM (PM_{10} and $PM_{2.5}$) concentrations (Figure 2). The experiment was carried out from 30 October to 1 November 2018, from 9:00 h to 17:00 h every day. All measured points covered various environmental spaces in the park. Wind speed and direction were recorded once per minute and particulate concentration was recorded every 20 minutes. It was sunny without significant pollution source changes during on-site measurements and there were no other human factors close to monitored points that would cause concentration changes.

During the experiment, prevailing wind direction at monitored point *A* was easterly, and maximum wind velocity reached 2.8 m/s (Figure 3a). Particle concentrations for the same period in the three-day experiment were averaged hourly. The mean hourly PM_{10} ranged between 297.3 and 427.2 µg/m^3 and the $PM_{2.5}$ ranged between 95.6 and 157.6 µg/m^3 (Figure 3b).
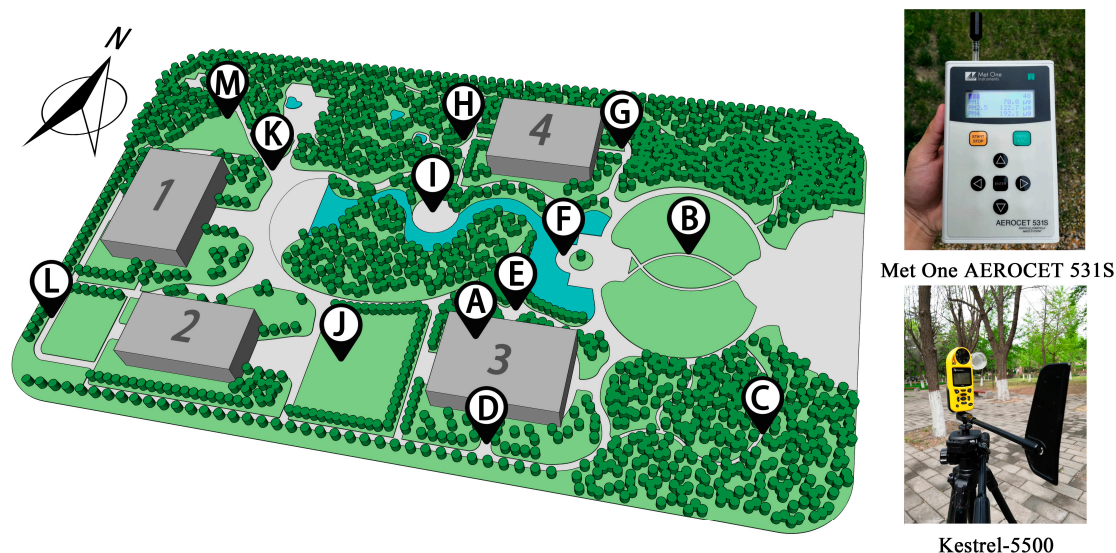

Figure 2. Photographs of test instruments and location of monitored points in the park.
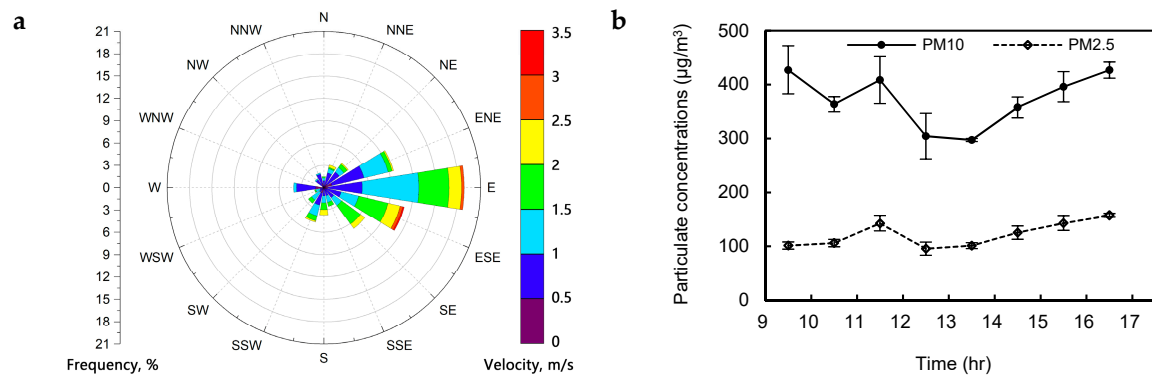
Figure 3. Wind rose (**a**) and hourly averaged PM concentrations (**b**) during on-site measurements.

2.3. Computational Approach

2.3.1. Model Setup

The simulation model was constructed by using the vegetation, buildings, water-filled pool and type of underlying surfaces parameters based on the present condition of the park (Figure 4). According to the established guidelines [66], the distance between the inlet (inflow boundary) and the target area was set to W (W is the width of the target site) and the distance from the target area to the outlet (outlet boundary) was set to 3W. The distance between the left/right symmetric boundary and the target area was W. The distance between top and the ground boundary was set to 11H (H is the height of buildings in the target area, H = 15 m). The computational domain, with a dimension of 1290 m × 675 m × 165 m, was divided into three types of structural hexahedral meshes (coarse meshes: $X_{min} = Y_{min} = Z_{min} = 0.27H$; fine meshes: $X_{min} = Y_{min} = Z_{min} = 0.13H$; and finest meshes: $X_{min} = Y_{min} = Z_{min} = 0.06H$).

The outlet boundary condition was established with fixed pressure and zero gradients. Rough wall functions were fixed for the ground boundary. Corresponding constant horizontal velocity and turbulent kinetic energy of the inflow profile were fixed at the top boundary, while the left and right symmetric boundary was modeled as a slippage wall without a gradient.
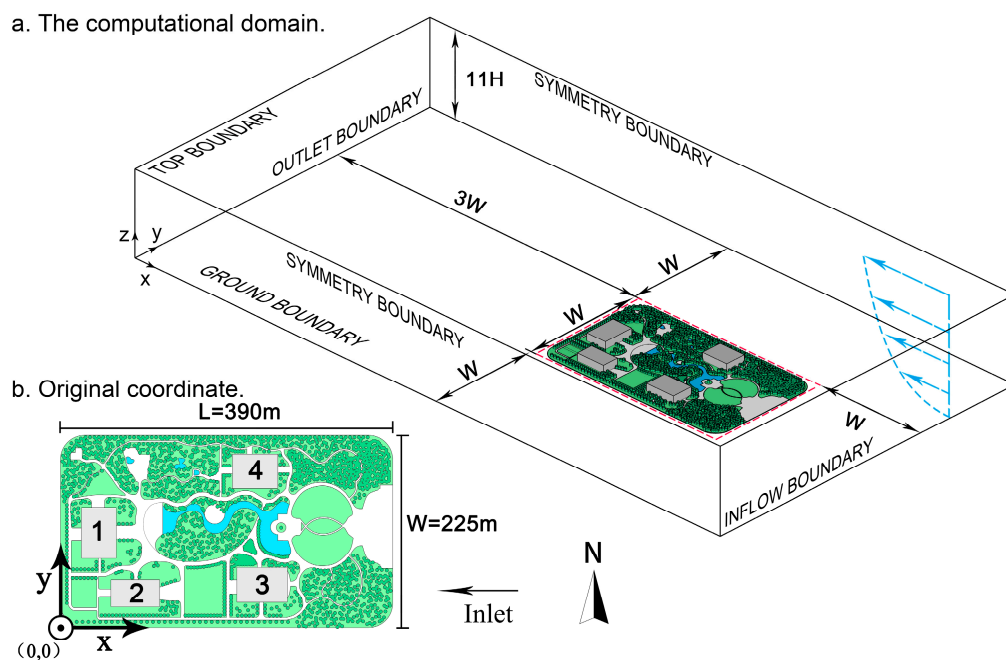

Figure 4. The computational domain.

The oncoming wind at the inlet is a gradient and is calculated using the equation:

$$u(z) = u_0(z/z_0)^\alpha.$$ (1)

where $u(z)$ is horizontal velocity at height z, and u_0 is the horizontal velocity at height z_0. In this model, $u_0 = 2.8$ m/s, $z_0 = 16.5$ m, and $\alpha = 0.25$ [67].

The turbulent kinetic energy, k (m^2/s^2), and its dissipation rate, ε (m^2/s^3), are set as:

$$k = \frac{u_*^2}{\sqrt{C_\mu}}\left(1 - \frac{z}{\delta}\right)$$ (2)

$$\varepsilon = \frac{u_*^3}{Kz}\left(1 - \frac{z}{\delta}\right)$$ (3)

where u_* is the friction velocity, δ is the depth of the boundary layer, and K is the von Karman's constant. In this model, $u_* = 0.52$ m/s, $K = 0.4$, and $C_\mu = 0.09$ [68].

Statistical data show that the predominant PM pollution sources in Xi'an in 2017 were mainly derived from atmospheric transportation [69]. To better replicate conditions during the on-site experiment, pollution sources were added to the inlet boundary in simulations. The average concentrations at monitored point A, which were added to the inlet boundary, were assumed to be constant. Particles in this domain were regarded as a continuum, and particle dispersion was assumed to have no effect on turbulence.

Trees in the model were parameterized as a one-dimensional column with a normalized LAD scaled to tree height [70]. LAD varied as a function of height modified by crown shape, height, and canopy edges. Different types of vegetation can be easily distinguished using non-uniform vertical distribution of LAD [71]. In this park, there are about 30 types of trees. To simplify computational simulations, six dominant species that account for more than 80% of vegetation were selected. Statistics on plant quantity, canopy diameter and height, and crown base height (m) of these trees were measured (Table 1). Leaf area index (LAI) of the major trees was measured using a LAI-2200C Plant Canopy Analyzer (LI-COR Inc., Lincoln, Nebraska) (m^2/m^2) with the corresponding LAD was calculated using Equation (7). All typical trees were parameterized with their calculated LAD profiles based on tree height, crown diameter, and crown base height. These data were then written into user-defined functions to characterize the three-dimensional canopy of trees in CFD simulations.

The deposition velocities of PM$_{2.5}$ and PM$_{10}$ on the foliage of typical trees, grass and a water-filled pool in the park are listed in Table 2 [24,38,49,52,72]. Previous research has found that particle deposition on building envelopes was less than 0.03%, which we considered to be negligible for this study [52].

Table 1. Typical vegetation parameters in the park.

Typical Plants	Crown Volume Expressions	X (m)	Y (m)	CBH (m)	LAD (m^2/m^3)
Pinus tabuliformis Carr.	$\pi x^2 y/12$	3.5	4	1.8	0.40
Platycladusorientalis (L.) Franco	$\pi x^2 y/12$	3.0	6.5	1.0	2.20
Ginkgo biloba L.	$\pi x^2 y/12$	2.6	9	2.0	1.26
Acer truncatum Bunge	$\pi x^2 y/6$	4.2	3.8	1.5	1.54
Populus tomentosa Carr.	$\pi x^2 y/4$	4.0	9.8	2.0	1.38
Sophora japonica L.	$\pi x^2 y/6$	3.5	6.0	2.0	2.06

Due to the age similarity among different tree categories in the park, mean canopy height, width and crown base height of plants is used. X—crown diameter, Y—crown height, CBH—crown base height.

Table 2. The deposition velocities of $PM_{2.5}$ and PM_{10} on the foliage of typical trees, grass, and water-filled pools.

Particle Size Fraction	Deposition Velocity (V_d)(m/s)							
	P. tabuliformis	*P. orientalis*	*G. biloba*	*A. truncatum*	*P. tomentosa*	*S. japonica*	**Grass**	**Pool**
PM_{10}	0.0279	0.0343	0.0371	0.0364	0.0057	0.0325	0.0064	0.0047
$PM_{2.5}$	0.0175	0.0458	0.0245	0.0922	0.0081	0.0454	0.0028	0.0001

2.3.2. Simulation Description

We reproduced airflow and particle diffusion using three-dimensional steady-state isothermal flow field models. CFD simulations were aligned with COST Action 732 parameters [73]. The RANS approach model, consisting of the *k-ε* Murakami-Mochida-Kondo (MMK) closure scheme, was used. This model was modified based on the standard *k-ε* model, which accurately reproduces airflow fields around buildings. The Semi-Implicit Method for Pressure-Linked Equations (SIMPLE) algorithm with the Quadratic Upstream Interpolation for Convective Kinematics (QUICK) discretization scheme was applied to all governing equations. The scaled iterative convergence criteria for all parameters in simulations were set to 10^{-6}. Simulations were run on an i7 2.67 GHz processor (Intel, Santa Clara, CA, USA). The Parabolic Hyperbolic or Elliptic Numerical Integration Code Series (PHOENICS; CHAM, London, UK, Edition: 2009) program was used to compute solutions.

In turbulence models, tree crowns are considered as a porous medium with individual tree branches are similar to the crown [74]. The drag and pressure produced by the tree crown decrease kinematic airflow energy. Therefore, resistance based on the momentum equation is considered to simulate vegetation influences on turbulence flow fields. The sink term is introduced to the momentum equation to express turbulence resistance by canopy layer:

$$S_{d,i} = -C_d \times LAD \times |U| \times u_i \tag{4}$$

where C_d is the drag coefficient, $|U|$ is the vector speed on foliage surface (m/s), and u_i. is the Cartesian velocity in *i* direction (m/s).

The LAD of vegetation is expressed by LAI, and defined as:

$$LAI = \int_0^h LAD \cdot dz \tag{5}$$

$$LAD = \alpha_m \left(\frac{h - z_m}{h - z} \right)^n exp \left[n \left(1 - \frac{h - z_m}{h - z} \right) \right] \tag{6}$$

where *h* is the average canopy height. When $0 \leq Z \leq Z_m$, $n = 6$ and $Z_m \leq Z \leq h$, $n = 0.5$. α_m is the maximum value of α at the perpendicular position Z_m. For computational efficiency, LAD is considered constant in the perpendicular direction and it can be calculated with canopy height and LAI:

$$LAD = LAI/h \tag{7}$$

The turbulence interaction between airflow and tree canopy can be expressed by additional source terms in momentum equation:

$$S_k = C_d \times LAD \times \left(\beta_p |U|^3 - \beta_d |U| k \right) \tag{8}$$

$$S_\varepsilon = C_d \times LAD \times \left(C_{4\varepsilon} \beta_p |U|^3 \frac{\varepsilon}{k} - C_{5\varepsilon} \beta_d |U| \varepsilon \right) \tag{9}$$

where β_p, β_d, $C_{4\varepsilon}$, and $C_{5\varepsilon}$ are empirical constants, β_p denotes the mean fluid kinetic energy of wake flow K which is produced by drag force of canopy, and β_d represents the K kinetic energy that is dissipated by the short circuits of Kolmogorov energy gradients. In the present study, β_p and β_d as well as the closure constants $C_{4\varepsilon}$ and $C_{5\varepsilon}$ are 1.0, 3.0, 1.5, and 1.5, respectively [75–77].

The revised generalized drift flux model considers the slippage between particulates and fluid (air) phase. It is a corrected Eulerian model that regards particles as a continuum when solving the conservation equation of PM mass/quantity concentration, and is widely applied due to its simulation accuracy and efficiency. In the revised generalized drift flux model, three dimensional tree models enhance PM deposition through turbulence diffusion. Tree branches and leaves also absorb PM, and some PM might be suspended on leaves or washed away [22]. The aerodynamic and deposition effects of plants on PM are expressed by additional source terms (S_{sink} and $S_{resuspension}$). In this way, the revised generalized drift flux model can comprehensively and accurately describe and simulate plants' influence on PM dispersion in real environments [20]. This model can be expressed as:

$$\frac{\partial\left[\left(V_j + V_{slip,j}\right)C\right]}{\partial x_j} = \frac{\partial}{\partial x_j}\left[\varepsilon_p\frac{\partial C}{\partial x_j}\right] + S_c - S_{sink} + S_{resuspension} \tag{10}$$

Particle slippage velocity (V_{slip}) is defined by gravity, thermal force by the thermophoresis effect, particle fluctuation defined by turbulence and particle acceleration [78], and is calculated as:

$$V_{slip,j} = \tau_p g_j + \tau_p \sum F_j + \frac{\tau_p}{C}S_{mj} - \frac{\tau_p}{C}\frac{\partial\left(V_{Pj}V_{pi}C\right)}{\partial x_i} \tag{11}$$

$$S_{mj} = \frac{\partial}{\partial x_i}\left[\varepsilon_p C\left(\frac{\partial V_{pj}}{\partial x_i} + \frac{\partial V_{pi}}{\partial x_j}\right)\right] + \left[\frac{\partial}{\partial x_i}\varepsilon_p\left(V_{pi}\frac{\partial C}{\partial x_j} + V_{pj}\frac{\partial C}{\partial x_i}\right)\right] \tag{12}$$

$$\tau_p = \frac{C_c\rho_p d_p{}^2}{18\mu} \tag{13}$$

where V_j and $V_{slip,j}$ are mean fluid (air) velocity and gravitational settling velocity of particles in direction j (m/s). C is particle concentration at the inlet (μg/m^3). ε_p is turbulent diffusivity (m^2/s), and that can be simplified to 1.0 [78]. S_c is the formation rate of particle sources (kg/m^{3}s). S_{sink} is the mass of particle absorbed by vegetation per cubic meter within a unit of time (μg/m^3). $S_{resuspension}$ is the secondary pollutant generated by foliage per cubic meter within a unit of time [79]. V_{pj} and V_{pi} are particle velocities in j and i directions (m/s), respectively. τ_p is the particle relaxation time. g_j is the gravitational acceleration in j direction (m/s^2). ΣF_j is the resultant force exerted upon the particle (m/s^2). S_{mj} is the momentum source of particle in j direction kg/(m^2 s^2). μ is molecular kinematic viscosity of air(Ns/m^2). ρ_p is density of atmospheric particles (kg/m^3). d_p is particle diameter (m). C_c is the Cunningham factor induced by slippage.

The effect of tree canopies on absorbing atmospheric particles is dependent on their LADs, deposition velocities and particulate concentrations in atmosphere, expressed as:

$$S_{sink} = LAD \times V_d \times C \tag{14}$$

The resuspension of particulate matter, as a term of volume source, is described as:

$$S_{resuspension} = S_{sink} \times P_{resuspension} \tag{15}$$

$$P_{resuspension} = -0.00041v^2 + 0.017v - 0.0016 \tag{16}$$

where V_d is particle deposition velocity on foliage (m/s); $P_{resuspension}$ is the percentage of resuspended particles [79]; v is the magnitude of air velocity (m/s).

2.4. Case Description

To understand the influence of vegetation coverage on particulate concentration distributions in the park, the total vegetation coverage ratio was set to 70% (including tree coverage ratio and tree clearing ratio). This is the standard for vegetation coverage ratio in parks [80]. Tree coverage ratio, *CVC*, and roof greening were chosen as three variables, and their influences on particulate concentration distributions in the park were analyzed. The *CVC* is expressed as [61]:

$$CVC(m^3/m^2) = \frac{\text{Total crown volume in measurement site}(m^3)}{\text{Area of measurement site }(m^2)} \tag{17}$$

Twelve scenarios were examined to meet simulation targets. Scenario 0 was the present condition of the park. Scenario 1 was the control group. Scenarios 3, 5, and 7 had different tree coverage ratios. Scenarios 2, 4, 6, and 8 had various *CVCs* by changing different types of tree canopy heights. Scenarios 9 and 10 had different pool coverage. Scenarios 10 and 11 were set with and without greening roof (Table 3).

Table 3. Case settings in numerical simulations.

Scenario	Area Coverage Proportion (%)						CVC (m³/m²)
	Tree Coverage	Tree Clearing	Pool Coverage	Hard Paving	Building Coverage	Total	
0 (Status quo)	25	50	5	10	10	100	1.15
1	-	-	-	90	10	100	-
2	5	65	-	20	10	100	0.1
3	60	10	-	20	10	100	2.4
4	60	10	-	20	10	100	3.6
5	30	40	-	20	10	100	1.2
6	30	40	-	20	10	100	1.8
7	15	55	-	20	10	100	0.6
8	15	55	-	20	10	100	0.9
9	30	40	10	10	10	100	1.2
10	30	40	5	15	10	100	1.2
11	30	40	5	15	10 (Green roofs)	100	1.2

3. Results and Discussion

3.1. Results of Model Evaluation

The accuracy of the airflow field and particle dispersion from the CFD simulation must be validated before the correct estimate the deposition effect of trees on particulate concentrations could be calculated. Simulations were based on the present conditions of the park. This enables the actual environment of the park (scenario 0) to be reproduced overlain by three grids (coarse meshes: $X_{min} = Y_{min} = Z_{min} = 0.27H$, fine meshes: $X_{min} = Y_{min} = Z_{min} = 0.13H$, and finest meshes: $X_{min} = Y_{min} = Z_{min} = 0.06H$). Specific-hour concentrations (PM$_{2.5}$ = 132 and PM$_{10}$ = 358 μg/m³), wind velocity (2.1 m/s) and wind direction (easterly) recorded at 14:30 h on 1 November 2018 were added in the inlet boundary. Three grid densities perform similar changing tendency of particle concentration and wind speed along the middle line (Figure 5). Grid independence was evaluated using the grid convergence index [81]. The grid convergence index between coarse and fine meshes was 4.61%, and was 3.87% between fine and the finest meshes that all meet the calculation requirements (<5%) [82]. Since an increase in the total grids could take more computational time, the above results indicate that the satisfactory grid independence may be archived by using fine meshes. Computations require only 49 hours and the accuracy is higher than with coarse meshes. Therefore, fine meshes were chosen in subsequent simulations of other scenarios (1–11).
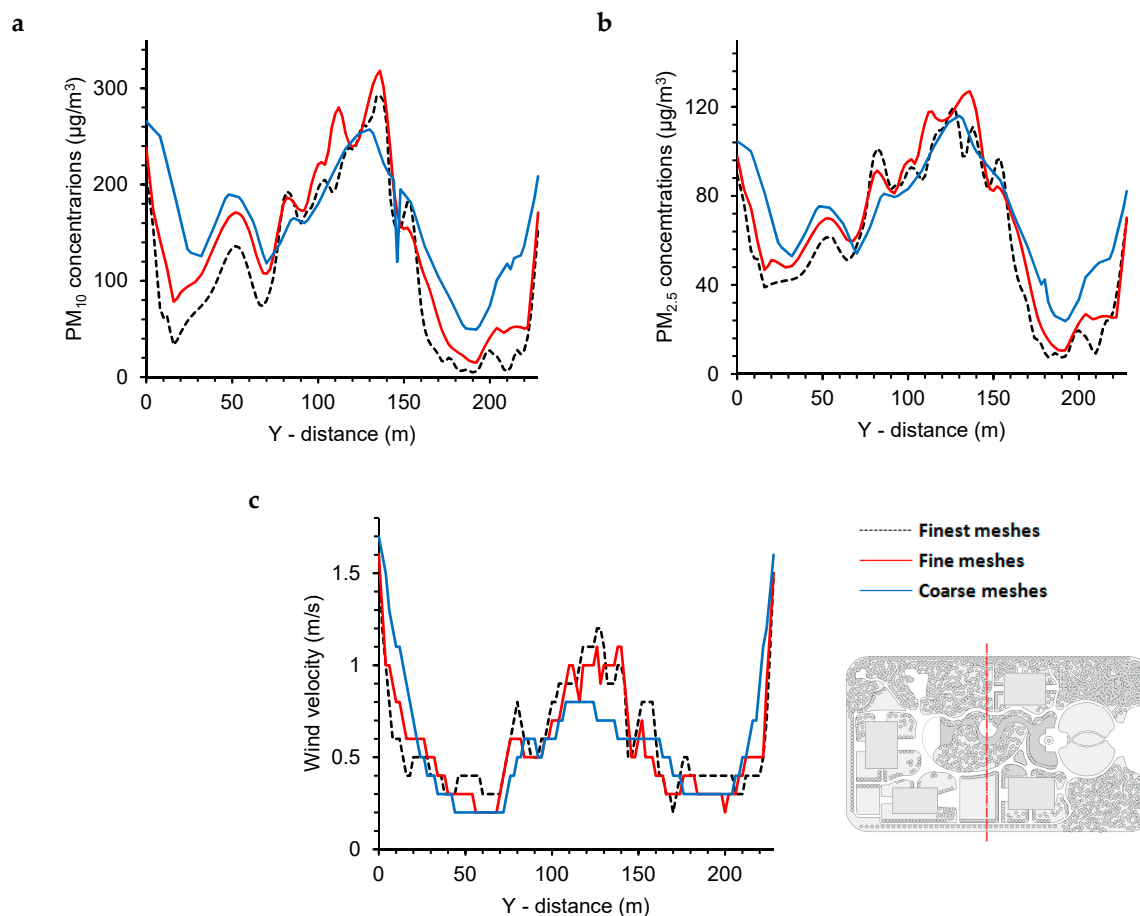
Figure 5. Predicted PM_{10} (**a**), $PM_{2.5}$ (**b**), and wind velocity (**c**) at the pedestrian level ($Z = 1.5$ m) along the middle line at $X = 180$ m for three different grid densities.

Figure 6 depicts a comparison of the CFD predictions with measured PM_{10}, $PM_{2.5}$, and wind velocity at different monitoring locations on 1 November. Each data point denotes the specific-time value recorded at 14:30 h. The standard deviations of PM_{10}, $PM_{2.5}$, and wind velocity were 70.9 μg/m^3, 30.9 μg/m^3, and 0.49 m/s. Overall, the linear regression of PM_{10} and $PM_{2.5}$ between CFD predictions and measurements all showed similar tendencies with a slope close to 1 and an R^2 greater than 0.94. The PM_{10} concentration difference between simulation and measurement was less than 20%. Differences of $PM_{2.5}$ concentration were less than 10% except that at point *D*. Point *D* was close to edge of the park and adjacent to roads where $PM_{2.5}$ might be higher due to vehicle emission particulates, although we scheduled field experiments for times when traffic volume were less. It is noteworthy that the correlation between simulated and measured $PM_{2.5}$ is stronger than that of PM_{10}. In the simulation process, we hypothesized that particulates diffuse with airflow, and the mutual frictional force and drag among particulates are negligible. The friction and resistance between the larger size particles are greater, which makes the difference of PM_{10} slightly larger than $PM_{2.5}$. The predicted wind velocities in windward regions (points *G* and *E*) agreed well with the measured data with discrepancies less than 10%. While velocities in leeward regions (points *H* and *J*) generally differed up to approximately 20% between the simulated and measured values due to blockage from buildings and trees. It also can be noticed that the simulated wind velocity at the monitored point of C deviated from that of measured data by 30.7%, owing to the CFD model used in our study was a RANS model including the *k-ε* MMK turbulence closure scheme, which was modified form the standard *k-ε* model and had better applicability to simulate airflow around buildings. Although previous studies indicated that Reynolds Stress Model (RSM) and Large Eddy Simulation (LES) reproduced better aerodynamic effect of plants compared with *k-ε* model [83], regarding validation of deposition model, we only considered the work

in which *k-ε* model was employed [84]. Thus, the monitored points surrounded by dense trees or far away from buildings exerted relatively large variations between simulated and measured data.
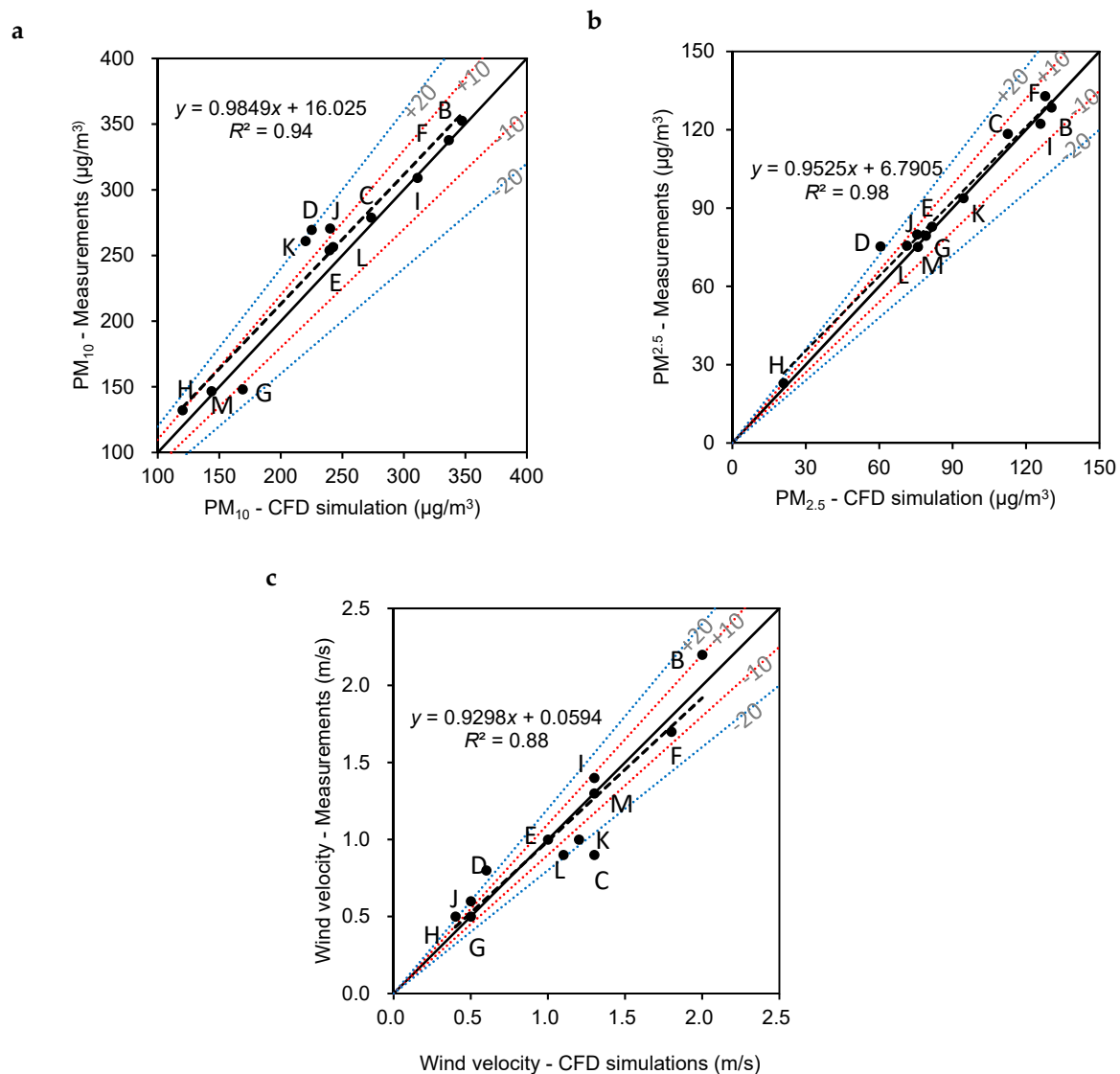

Figure 6. Comparison of simulation results with measured data for PM_{10} (**a**), $PM_{2.5}$ (**b**), and wind velocity (**c**) of various monitoring points (The solid black line represents a slope of 1, and the dotted line is a fit curve between simulations and experiments).

3.2. Tree Coverage Ratio (%)

The concentration in the windward areas of the park was significantly higher than that in the leeward. With the increase of tree coverage ratio, PM_{10} ($PM_{2.5}$) decreased significantly, and the concentration in the downwind areas was more variable than that in upwind areas. When the tree coverage ratios were rising from 15% (Scenario 7), 30% (Scenario 5), to 60% (Scenario 3), the concentration in the leeward areas of buildings decreased significantly, while the difference of concentration on windward areas of buildings was small (Figure 7). Due to building obstruction, PM_{10} and $PM_{2.5}$ on leeward areas of buildings at the pedestrian level were small, but concentrations on the windward areas of buildings were relatively high, agreeing well with the results of Ji and Zhao (2014) [20]. In areas where trees were planted, the pedestrian-level concentration was clearly lower. Minimum concentrations in the park all occurred in the large-scaled tree planting areas. Concentrations close to the tree canopy were relatively low and decreased the concentration significantly at the pedestrian level.

This pattern matches previous results [85,86], however, some studies demonstrated that concentrations at the tree canopy level were higher in the street canyons [50,53,87]. This appears to be caused by different pollution sources, for instance internal (e.g. traffic-emitted), rather than external sources transmitted from atmosphere as in our study. The reduction in ventilation was also responsible for the buildup of pollutants in street canyons. Additionally, these studies largely considered the aerodynamic effect of trees on pollutants, and the absorption effect was not fully taken into account. A previous study demonstrated that when the average wind speed was 5 m/s, trees could decrease $PM_{2.5}$ concentration by 4.6% through deposition and only 0.7% through aerodynamic effects [88].
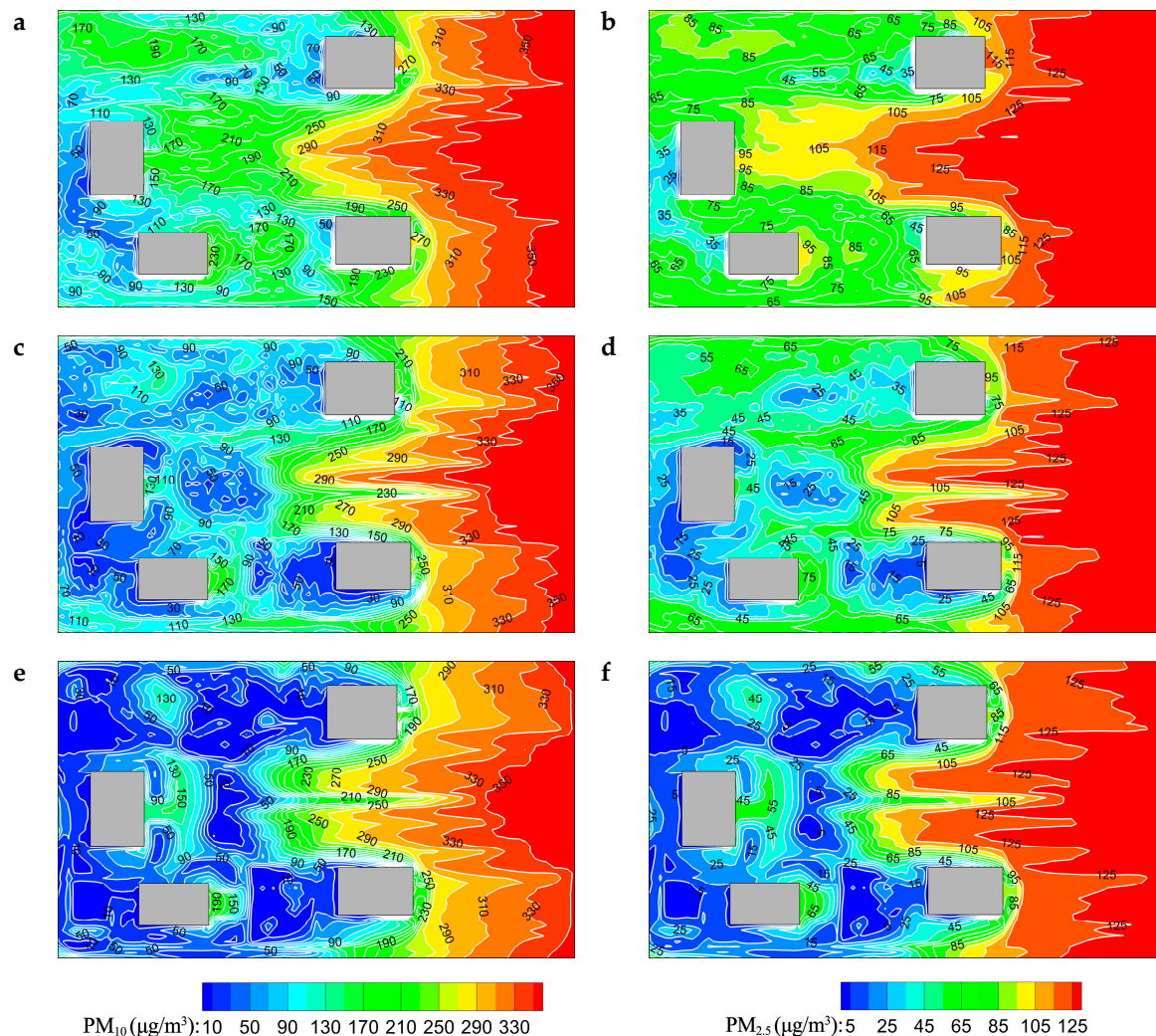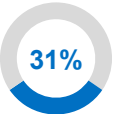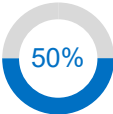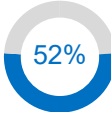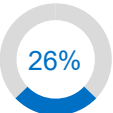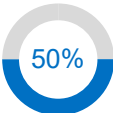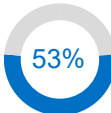

Figure 7. PM_{10} (left panel) and $PM_{2.5}$ (right panel) concentration distributions for tree coverage ratios of 15% (**a**,**b**), 30% (**c**,**d**), 60% (**e**,**f**) at 1.5 m height.

To compare our results against the World Health Organization air quality guidelines (WHO AQGs), our study chose interim target-1 (IT-1) for $PM_{2.5}$ and PM_{10} with 24 hour average concentrations of 75 and 150 $\mu g/m^3$ as a criterion [89]. An increase in tree coverage ratio from 15% to 30% resulted in area proportion with pedestrian-level $PM_{2.5}$ less than 75 $\mu g/m^3$ increasing from 26% to 50%, and area proportion with pedestrian-level PM_{10} less than 150 $\mu g/m^3$ increasing from 31% to 50%. However, this trend was not obvious when the tree coverage ratio increased from 30% to 60%. The area proportion with pedestrian-level $PM_{2.5}$ less than 75 $\mu g/m^3$ only increased from 50% to 53%, and the area with pedestrian-level PM_{10} less than 150 $\mu g/m^3$ only increased by 2% (Table 4).

Table 4. The area proportion with pedestrian-level PM_{10} and $PM_{2.5}$ met the WHO criterion when the tree coverage ratios are 15%, 30%, and 60%.

Criterion	Tree Coverage Ratio (%)		
	15 (Scenario 7)	30 (Scenario 5)	60 (Scenario 3)
$PM_{10} \leq 150$ µg/m^3	31%	50%	52%
$PM_{2.5} \leq 75$ µg/m^3	26%	50%	53%

To quantitatively investigate the effect of tree coverage ratio on particulate concentrations in the pedestrian space, the average concentration (1.5 m height) as a function of tree coverage ratio is displayed in Figure 8. To generalize the results, the concentrations at different tree coverage ratio were normalized by the concentrations at the inlet. The fitting curve of PM_{10} was lower than that of $PM_{2.5}$. This is mostly due to turbulent diffusion and surface deposition reduction intensified by increasing tree coverage ratio, and larger size particles were easier to be deposited on leaf surfaces. At tree coverage ratio = 10%, the $PM_{2.5}$ was approximately 80% of the inlet concentrations, while PM_{10} was 72% of the inlet value. At tree coverage ratio = 30%, the concentrations declined to approximately 62% ($PM_{2.5}$) and 50% (PM_{10}) of the inlet values. When the tree coverage reached 60%, the concentrations declined to approximately 50% ($PM_{2.5}$) and 40% (PM_{10}) of the inlet values. By substituting $y = 75$ µg/m^3 in equation $y = [1.177 - 0.17\ln(x)] \times C_{in}$. It can be seen that when tree coverage ratio >38.1%, the pedestrian-level $PM_{2.5}$ could conform to the WHO AQGs (IT-1) standards.
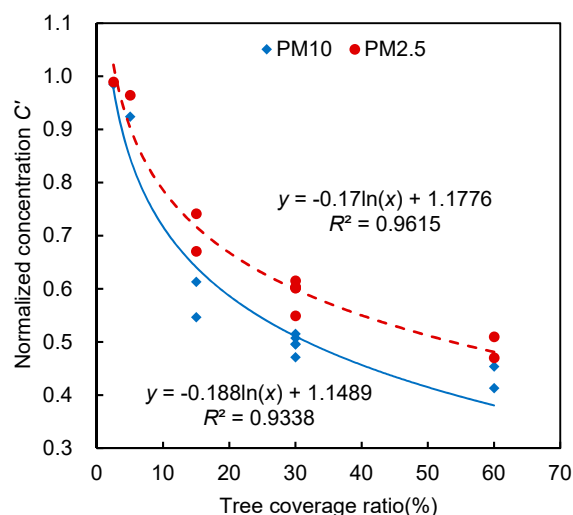

Figure 8. Relationships between tree coverage ratio and normalized concentration at 1.5 m height. $C' = C_x/C_{in}$, C_x is the concentrations at different tree coverage ratio, C_{in} is the concentration added at inlet boundary ($C_{in} = 132$ µg/m^3 for $PM_{2.5}$ and 358 µg/m^3 for PM_{10}).

3.3. Crown Volume Coverage (CVC)

PM_{10} and $PM_{2.5}$ under *CVCs* = 1.2 (Scenario 5) and 1.8 m^3/m^2 (Scenario 6) were compared when the tree coverage ratio was 30% (Figure 9). The concentration in the space between two windward buildings (Bldgs.3 and 4) was relatively high. The concentrations decreased sharply when they flow with air and diffuse to areas where trees were planted. Under the two *CVC* conditions, the concentration on windward surface of buildings was relatively high, but the concentration on tree planted regions

and leeward surface of buildings was relatively low. When *CVC* increased from 1.2 to 1.8 m³/m², the PM$_{10}$ and PM$_{2.5}$ decreased significantly. The WHO interim target-1 (IT-1) for PM$_{2.5}$ and PM$_{10}$ with 24 h average concentrations was also selected as a criterion. When the *CVC* increased from 1.2 to 1.8 m³/m², the area proportion with pedestrian-level PM$_{2.5}$ less than 75 µg/m³ increased by 2% (from 48% to 50%), while the area with pedestrian-level PM$_{10}$ less than 150 µg/m³ increased from 47% to 51% (Table 5).
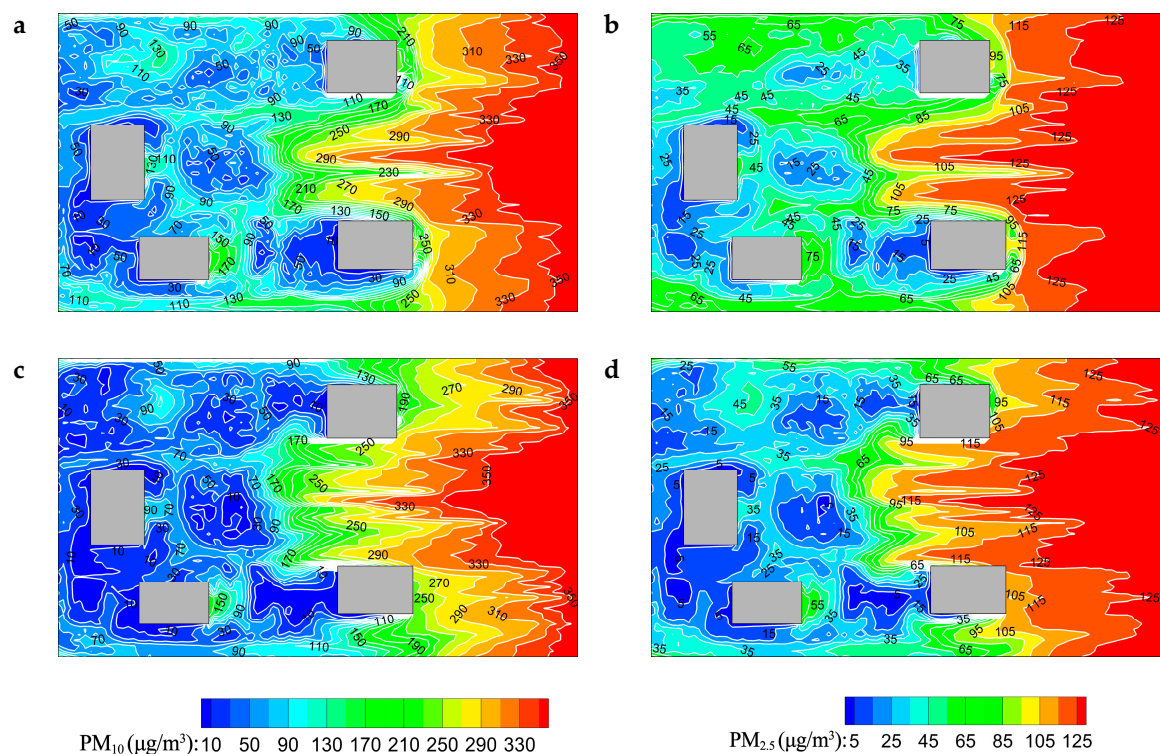

Figure 9. PM$_{10}$ (left panel) and PM$_{2.5}$ (right panel) concentration distributions for *CVC*s of 1.2 m³/m² (**a**,**b**) and 1.8 m³/m² (**c**,**d**) at 1.5 m height.

Table 5. The area proportion with pedestrian-level PM$_{10}$ and PM$_{2.5}$ met the WHO criterion when the *CVC*s are 1.2 and 1.8 m³/m².

Criterion	CVC (m³/m²)	
	1.2 (Scenario 5)	1.8 (Scenario 6)
PM$_{10}$ ≤ 150 µg/m³	47%	51%
PM$_{2.5}$ ≤ 75 µg/m³	48%	50%

The results and curve fitting between the average concentration (1.5 m height) and *CVC* are shown in Figure 10. The correlation between PM$_{2.5}$ and *CVC* was stronger than that of PM$_{10}$. The average concentration was found to decline exponentially with increasing *CVC*. This is consistent with the findings of Wu et al. (2018) [90]. The difference in concentration between PM$_{2.5}$ and PM$_{10}$ was initially small at *CVC* = 0.2 m³/m² and gradually increased towards *CVC* = 3.5 m³/m². This is a result of increased surface deposition mostly due to turbulent diffusion with increasing *CVC*. At *CVC* = 0.5 m³/m², the PM$_{2.5}$ was approximately 75% of the inlet concentration, while the

concentration of PM$_{10}$ was 70% of the inlet value. Concentrations are significantly reduced with the increase of *CVC* from 0 to 2.0 m^3/m^2. A break-even point was observed at *CVC* = 2.6 m^3/m^2 where the particle concentration declined to the same level (50% of the inlet concentration). By substituting $y = 75$ µg/m^3 in equation $y = [0.66 - 0.17\ln(x)] \times C_{in}$. The WHO AQGs (IT-1) specify that the *CVC* should be greater than or equal to 1.83 m^3/m^2.
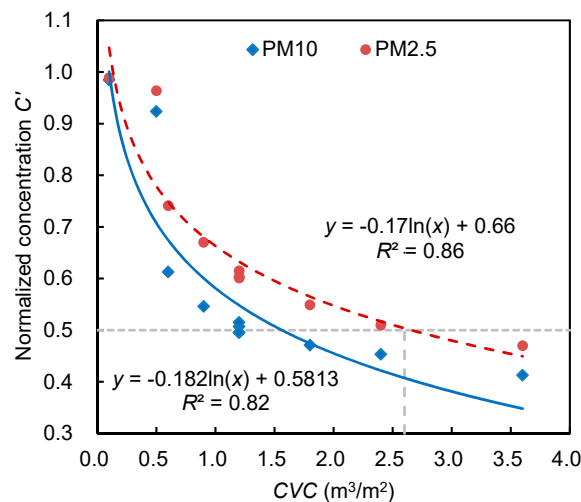

Figure 10. Relationships between *CVC* and normalized concentration at 1.5 m height. $C' = C_x/C_{in}$, C_x is the concentrations at different *CVC*, C_{in} is the concentration added at inlet boundary (C_{in} = 132 µg/m^3 for PM$_{2.5}$ and 358 µg/m^3 for PM$_{10}$).

3.4. Greening Roof

Research demonstrates that indoor PM is significantly correlated with outdoors, and outdoor PMs mainly enter indoor spaces through transmission and penetration [91–93]. Therefore, the windward building (Bldg.4) and leeward building (Bldg.2) were chosen to analyze influences of roof greening on concentration close to building walls (0.5 m away from the building facade). Concentrations with and without roof greening were compared (Figure 11).

The concentration on windward facade of a building was significantly higher than that on the leeward facade. Concentrations gradually increased with height above the tree canopy, consistent with the results of Ji and Zhao (2014) [20]. It is clear in Figure 11a,b that the deposition effect of roof greening around the leeward façade (the difference between blue solid and dotted lines) was stronger than that of windward facade. The concentration on south facade of Bldg.4 (facade D) was higher than that on north one (facade A). Since the south wall was close to the ventilation corridor, particulate concentration in this region was relatively high. Concentration differences between the south and north facades of Bldg.2 were small. In Bldg.4, the concentration in the lower building space (height < 12 m) was higher with greening roof, but the concentration in the upper building space (height > 12 m) decreased significantly. PM$_{10}$ and PM$_{2.5}$ were respectively reduced by maximum values of 9.7 and 4.5 µg/m^3. In Bldg.2, roof greening could decrease the concentration around each façade at different heights. Roof greening unsurprisingly appears to reduce roof level particulate concentrations more effectively. The maximum reductions of PM$_{10}$ and PM$_{2.5}$ were 40.4 and 13.8 µg/m^3, respectively. Greening roof thus significantly reduced particulate concentration around facades of leeward buildings.

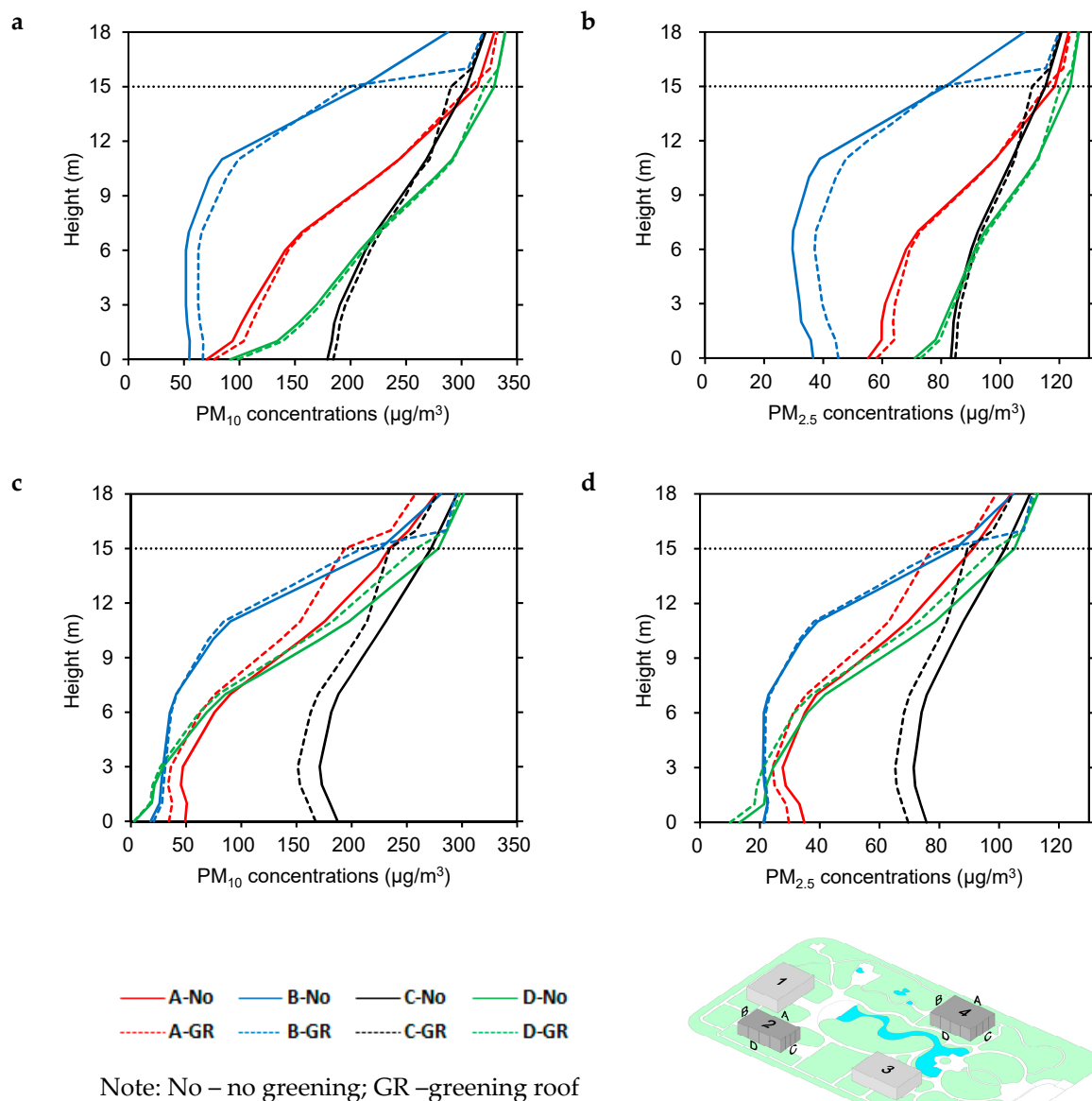**Figure 11.** Comparison of vertical PM$_{2.5}$ and PM$_{10}$ around the facades of Bldg.4 (**a**,**b**) and Bldg.2 (**c**,**d**) with greening roofs and no greening.

The temporal mean concentration at 1.5 m height above the tops of buildings with roof greening was lower than that without roof greening (Figure 12). The concentration with roof greening varied over a larger range, but was smaller than without greening. The median concentration with roof greening was lower than that without roof greening. We found that the difference between the median and the upper (lower) quartiles was smaller, indicating that particle concentration above roof was discrete with roof greening. Roof greening can further reduce particulate concentration at the top of leeward buildings (Bldg.2), and the average reductions of PM$_{10}$ was 7% and of PM$_{2.5}$ was 5%.

Particulate matter disperses within the airflow field. Roof greening above the windward building hinders airflow, causing PMs to increase in the lower layers of the windward building. Planting vegetation on the roof of the windward building, although it reduced the concentration near the upper level, is still not desirable. Thus, greening roof on leeward buildings, due to their relatively low wind speed, particles were easily deposited on leaf surfaces. Therefore, greening roofs should be used in an appropriate space, and greening roofs on leeward buildings are more effective and a better choice to reduce particles.
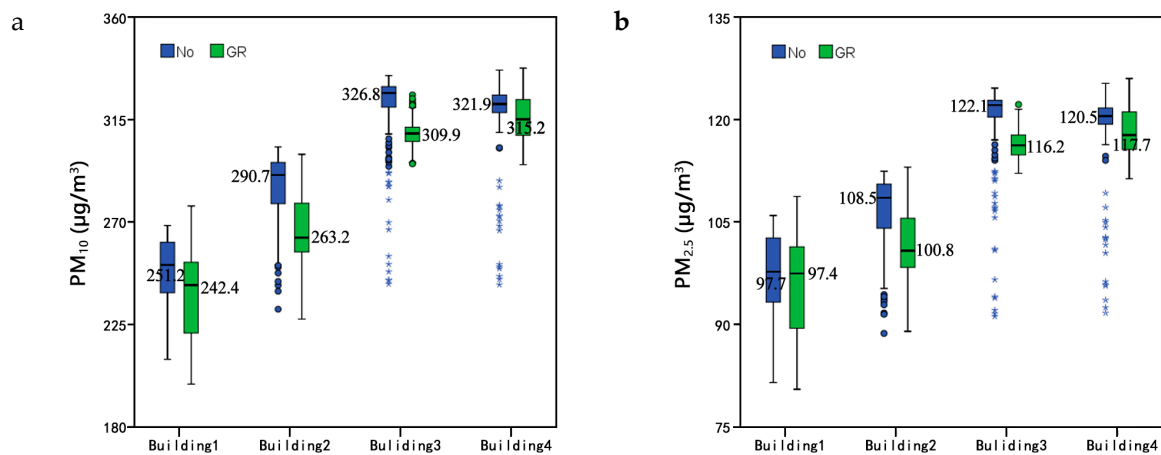
Figure 12. Comparison of averaged PM_{10} (**a**) and $PM_{2.5}$ (**b**) at 1.5 m above the top of the buildings with (green bars) and without (blue bars) green roofs.

3.5. Removal Rate

Tree coverage and *CVC* are significant predictors of particulate concentration distributions. In this section, the influence of tree coverage and *CVC* on the average particulate concentration at the pedestrian level was investigated. The reduction rate of particulate concentration was calculated as:

$$\omega = (C_{ave,no\ greenery} - C_{ave})/C_{ave,no\ greenery} \tag{18}$$

where ω is the removal rate capability of greenery on PM_{10} and $PM_{2.5}$. $C_{ave,non-greenery}$ and C_{ave} are the average particulate concentrations at the pedestrian level with and without greenery.

Removal rates of pedestrian-level PM_{10} and $PM_{2.5}$ are positively related to both tree coverage ratio and *CVC* ($R^2 > 0.90$) (Figure 13). An increase in tree coverage ratio from 0 to 30%, reduced concentration sharply. An increase in *CVC* from 0 to 1.8 m^3/m^2, greatly decreased particulate concentration. This pattern agrees well with an experiment conducted in a Shanghai park [61]. Further increasing of tree coverage and *CVC* do not appear to have significant mitigating effect on particles. When trees are very abundant, there is airflow resistance and this obstruction of atmospheric circulation increases the local particles. So that removal rate stabilizes when *CVC* > 1.8 and tree coverage ratio >30%. From these results, we can concluded that number of trees planted in a park is not simply the more the better. The most economical and reasonable tree coverage ratio and *CVC* should be 30% and 1.8 m^3/m^2.
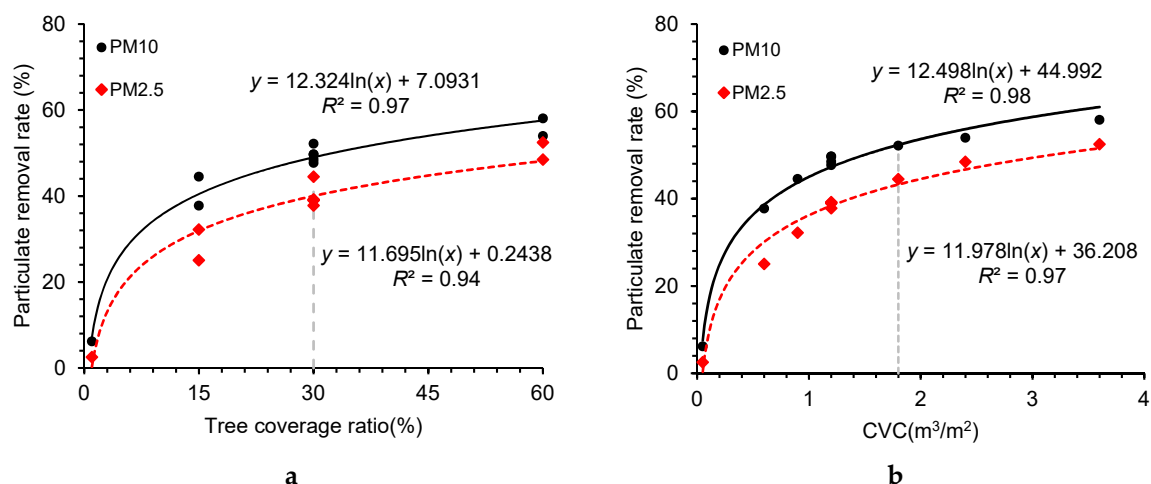

Figure 13. Regression analysis between tree coverage ratio (**a**), *CVC* (**b**) and particulate removal rate.

In this study, the influence of vegetation enhancement on PM dispersion in an urban park was analyzed. Results demonstrate the utility of PM removal rate corresponding to tree coverage ratio and *CVC* as supplementary indices in urban park design. However, our investigations uncovered some limitations: (1) We only simulated airflows and PM dispersion with a single wind direction. However, real-world meteorological changes are complex and, thus, future studies should focus on multi-perspective simulation analysis with more complex meteorological parameters, i.e., different pollution levels, wind speed and direction, park spatial scale. (2) Pollution sources were assumed to dilute through the inlet boundary in this study, while internal pollution sources and regional traffic pollution were not taken into account. Our simulation hypothesized that particulate diffusion was continuous, without the influence of unsteady-state airflow changes. In practice however, airflow changes continuously and even steady-state airflow influences particulate diffusion. More experiments could verify these effects. (3) Actual green spaces in parks are generally arbor-shrub-grass structures. This study only considered the impact of trees. Future studies should include the comprehensive effects of more complex arbor-shrub-grass structure to improve the prediction accuracy for actual urban environments. (4) Vegetation growth is dynamic and the effects of vegetation on dust retention during different growth periods differed significantly in our simulations. Hence, our conclusions should be verified with field data. (5) Finally, effects of solar radiation, heat transmission among buildings, vegetation, water and underlying surfaces on particulate diffusion were not accounted for but should be considered to make simulations more realistic.

4. Conclusions

The objective of this study was to investigate the effects of supplementary green areas and associated coverage ratios on $PM_{2.5}$ and PM_{10} concentration distributions in an urban park. Numerical simulations and field measurements were performed to examine the aerodynamic and deposition effects of trees on PM dispersion, which would provide architects and planners with a better understanding of the effect of park design on air quality by probing the impacts of changing *CVC*, tree coverage ratio, and supplementary green areas on atmospheric PM reduction. The primary results were summarized as follows:

(1) Field data and simulations were strongly correlated in a simplification of the vegetation model ($R^2 > 0.88$), indicating that the model could reflect the real influence of trees on particulate concentration distributions in the park.

(2) Assuming that pollution sources were diluted through the inlet boundary, the tree coverage ratio and *CVC* were the primary factors affecting PM dispersion. To ensure pedestrian-level $PM_{2.5}$ meets the standards of WHO AQGs (IT-1), tree coverage ratio should be greater than 37.8%, and *CVC* should be greater than 1.8 m^3/m^2.

(3) Roof greening can reduce particulate concentration at the top of the building. Particulate concentrations on vertical spaces and roofs of leeward buildings were lower than that of windward buildings. The average reduction ratio above the roof of a leeward building for PM_{10} was 7% and for $PM_{2.5}$ was 5% comparing greening and non-greening roof.

(4) When the tree coverage ratio increased from 0 to 30% and *CVC* increased from 0 to 1.8 m^3/m^2, the PM reduction ratio increased significantly. These patterns remain stable as the tree coverage ratio and *CVC* continued to increase.

Our study shows that vegetation can absorb atmospheric PM directly in a tree canopy, and indirectly through ventilation. Therefore, urban park solutions are not simply the more the better, because trees can dampen ventilation. To improve particle reduction and save resources, the most economical and reasonable tree coverage ratio should be 30% and *CVC* should be 1.8 m^3/m^2. When the roof is greened, vegetation should be planted on leeward buildings instead of windward buildings to remove more PM around building. These findings provide a useful strategy with the implementation of greening modifications in urban parks to mitigate atmospheric pollution.

Nomenclature

C	particle concentration at the inlet	$V_{slip,j}$	gravitational settling velocity of particles in j direction
C_c	Cunningham factor induced by slippage	V_{pj}	particle velocities in j directions
$C_{4\varepsilon}$	empirical constant, 1.5	V_{pi}	particle velocities in i directions
$C_{5\varepsilon}$	empirical constant, 1.5	d_p	particle diameter
CBH	crown base height	h	average canopy height
C_d	drag coefficient of plant elements	u_i	Cartesian velocity in i direction
CVC	crown volume coverage	k	turbulent kinetic energy
C_μ	turbulent constant, 0.09	u_*	friction velocity
GR	greening roof	$u(z)$	horizontal velocity at height z
K	von Karman's constant, 0.4	u_o	horizontal velocity at height z_0
LAD	leaf area density	v	magnitude of air velocity
LAI	leaf area index	β_p	mean fluid kinetic energy of wake flow K that is produced by drag force of canopy, 1.0
PM	particulate matter	β_d	kinetic energy that is dissipated by short circuit of Kolmogorov energy gradients, 3.0
$P_{resuspension}$	percentage of resuspended particles	ε_p	turbulent diffusivity, 1.0
S_c	formation rate of particle sources	τ_p	particle relaxation time
$S_{d,i}$	source term of wind speed loss due to drag forces on plants	g_j	gravitational acceleration in j direction
S_k	turbulence generation	μ	molecular kinematic viscosity of air
S_ε	turbulence dissipation	ρ_p	atmospheric particle density
S_{sink}	mass of particle absorbed by vegetation	ω	particulate matter removal rate
$S_{resuspension}$	the secondary pollutant generated by foliage	α	power law index, 0.25
S_{mj}	momentum source of particle in j direction	ε	turbulent energy dissipation rate
$|U|$	vector speed on foliage surface	δ	boundary layer depth
V_d	deposition velocity	ΣF_j	resultant force exerted upon the particle
V_j	mean fluid (air) velocity in j direction		

References

1. Zhang, X.; Zhang, X.; Chen, X. Happiness in the air: How does a dirty sky affect mental health and subjective well-being? *J. Environ. Econ. Manag.* **2017**, *85*, 81–94. [CrossRef] [PubMed]
2. Chang, T.Y.; Zivin, J.G.; Gross, T.; Neidell, M. The effect of pollution on worker productivity: Evidence from call center workers in China. *Am. Econ. J. Appl. Econ.* **2019**, *11*, 151–172. [CrossRef]
3. Zheng, S.; Wang, J.; Sun, C.; Zhang, X.; Kahn, M.E. Air pollution lowers Chinese urbanites' expressed happiness on social media. *Nat. Hum. Behav.* **2019**, *3*, 237–243. [CrossRef] [PubMed]
4. Brunekreef, B.; Holgate, S.T. Air pollution and health. *Lancet* **2002**, *360*, 1233–1242. [CrossRef]
5. Karottki, D.G.; Spilak, M.; Frederiksen, M.; Andersen, Z.J.; Madsen, A.M.; Ketzel, M.; Massling, A.; Gunnarsen, L.; Møller, P.; Loft, S. Indoor and outdoor exposure to ultrafine, fine and microbiologically derived particulate matter related to cardiovascular and respiratory effects in a panel of elderly urban citizens. *Int. J. Environ. Res. Public Health* **2015**, *12*, 1667–1686. [CrossRef]
6. Magalhaes, S.; Baumgartner, J.; Weichenthal, S. Impacts of exposure to black carbon, elemental carbon, and ultrafine particles from indoor and outdoor sources on blood pressure in adults: A review of epidemiological evidence. *Environ. Res.* **2018**, *161*, 345–353. [CrossRef]

7. Nowak, D.J.; Hirabayashi, S.; Doyle, M.; McGovern, M.; Pasher, J. Air pollution removal by urban forests in Canada and its effect on air quality and human health. *Urban For. Urban Green.* **2018**, *29*, 40–48. [CrossRef]

8. Katsouyanni, K.; Touloumi, G.; Samoli, E.; Gryparis, A.; Le-Tertre, A.; Monopolis, Y.; Rossi, G.; Zmirou, D.; Ballester, F.; Boumghar, A.; et al. Confounding and effect modification in the short-term effects of ambient particles on total mortality: Results from 29 European cities within the APHEA2 project. *Epidemiology* **2001**, *12*, 521–531. [CrossRef] [PubMed]

9. Samet, J.M.; Dominici, F.; Curriero, F.C.; Coursac, I.; Zeger, S.L. Fine particulate air pollution and mortality in 20 U.S. cities, 1987–1994. *N. Engl. J. Med.* **2000**, *343*, 1742–1749. [CrossRef] [PubMed]

10. Schwartz, J. Is there harvesting in the association of airborne particles with daily deaths and hospital admissions. *Epidemiology* **2001**, *12*, 155–161. [CrossRef]

11. Beckett, K.P.; Freer-Smith, P.H.; Taylor, G. Urban woodlands: Their role in reducing the effects of particulate pollution. *Environ. Pollut.* **1998**, *99*, 347–360. [CrossRef]

12. Powe, N.A.; Willis, K.G. Mortality and morbidity benefits of air pollution (SO_2 and PM_{10}) absorption attributable to woodland in Britain. *J. Environ. Manag.* **2004**, *70*, 119–128. [CrossRef] [PubMed]

13. Rui, L.; Buccolieri, R.; Gao, Z.; Ding, W.; Shen, J. The impact of green space layout on microclimate and air quality in residential districts of Nanjing, China. *Forests* **2018**, *9*, 224. [CrossRef]

14. Irga, P.J.; Burchett, M.D.; Torpy, F.R. Does urban forestry have a quantitative effect on ambient air quality in an urban environment? *Atmos. Environ.* **2015**, *120*, 173–181. [CrossRef]

15. Nowak, D.J. Institutionalizing urban forestry as a "biotechnology" to improve environmental quality. *Urban For. Urban Green.* **2006**, *5*, 93–100. [CrossRef]

16. McDonald, A.G.; Bealey, W.J.; Fowler, D.; Dragosits, U.; Skiba, U.; Smith, R.I.; Donovan, R.G.; Brett, H.E.; Hewitt, C.N.; Nemitz, E. Quantifying the effect of urban tree planting on concentrations and depositions of PM_{10} in two UK conurbations. *Atmos. Environ.* **2007**, *41*, 8455–8467. [CrossRef]

17. Escobedo, F.J.; Nowak, D.J. Spatial heterogeneity and air pollution removal by an urban forest. *Landsc. Urban Plan.* **2009**, *90*, 102–110. [CrossRef]

18. Fantozzi, F.; Monaci, F.; Blanusa, T.; Bargagli, R. Spatio-temporal variations of ozone and nitrogen dioxide concentrations under urban trees and in a nearby open area. *Urban Clim.* **2015**, *12*, 119–127. [CrossRef]

19. Janhäll, S. Review on urban vegetation and particle air pollution—Deposition and dispersion. *Atmos. Environ.* **2015**, *105*, 130–137. [CrossRef]

20. Ji, W.; Zhao, B. Numerical study of the effects of trees on outdoor particle concentration distributions. *Build. Simul.* **2014**, *7*, 417–427. [CrossRef]

21. Gallagher, J.; Baldauf, R.; Fuller, C.H.; Kumar, P.; Gill, L.W.; McNabola, A. Passive methods for improving air quality in the built environment: A review of porous and solid barriers. *Atmos. Environ.* **2015**, *120*, 61–70. [CrossRef]

22. Ould-Dada, Z.; Baghini, N.M. Resuspension of small particles from tree surfaces. *Atmos. Environ.* **2001**, *35*, 3799–3809. [CrossRef]

23. Ould-Dada, Z. Dry deposition profile of small particles within a model spruce canopy. *Sci. Total Environ.* **2002**, *286*, 83–96. [CrossRef]

24. Freer-Smith, P.H.; Beckett, K.P.; Taylor, G. Deposition velocities to *Sorbus aria*, *Acer campestre*, *Populus deltoides* × *trichocarpa* 'Beaupré', *Pinus nigra* and × *Cupressocyparis leylandii* for coarse, fine and ultra-fine particles in the urban environment. *Environ. Pollut.* **2005**, *133*, 157–167. [CrossRef] [PubMed]

25. Mori, J.; Hanslin, H.M.; Burchi, G.; Sæbø, A. Particulate matter and element accumulation on coniferous trees at different distances from a highway. *Urban For. Urban Green.* **2015**, *14*, 170–177. [CrossRef]

26. Xie, C.; Kan, L.; Guo, J.; Jin, S.; Li, Z.; Chen, D.; Li, X.; Che, S. A dynamic processes study of PM retention by trees under different wind conditions. *Environ. Pollut.* **2018**, *233*, 315–322. [CrossRef] [PubMed]

27. Qiu, L.; Liu, F.; Zhang, X.; Gao, T. The reducing effect of green spaces with different vegetation structure on atmospheric particulate matter concentration in Baoji city, China. *Atmosphere* **2018**, *9*, 332. [CrossRef]

28. Baidurela, A.; Halik, Ü.; Aishan, T.; Nuermaimaiti, K. Maximum dust retention of main greening trees in arid land oasis cities, Northwest China. *Sci. Silvae Sin.* **2015**, *51*, 57–63.

29. Fan, S.Y.; Yan, H.; Qishi, M.Y.; Bai, W.L.; Pi, D.J.; Li, X.; Dong, L. Dust capturing capacities of twenty-six deciduous broad-leaved trees in Beijing. *J. Plant Ecol.* **2015**, *39*, 736–745.

30. Dzierżanowski, K.; Gawroński, S.W. Use of trees for reducing particulate matter pollution in air. *Chall. Mod. Technol.* **2011**, *2*, 69–73.

31. Przybysz, A.; Sæbø, A.; Hanslin, H.M.; Gawroński, S.W. Accumulation of particulate matter and trace elements on vegetation as affected by pollution level, rainfall and the passage of time. *Sci. Total Environ.* **2014**, *481*, 360–369. [CrossRef] [PubMed]

32. Sgrigna, G.; Sæbø, A.; Gawronski, S.W.; Popek, R.; Calfapietra, C. Particulate matter deposition on *Quercus ilex* leaves in an industrial city of central Italy. *Environ. Pollut.* **2015**, *197*, 187–194. [CrossRef]

33. Chen, L.X.; Liu, C.M.; Zou, R.; Yang, M.; Zhang, Z.Q. Experimental examination of effectiveness of vegetation as bio-filter of particulate matter in the urban environment. *Environ. Pollut.* **2016**, *208*, 198–208. [CrossRef] [PubMed]

34. Zhang, Z.D.; Xi, B.Y.; Cao, Z.G.; Jia, L.M. Exploration of a quantitative methodology to characterize the retention of $PM_{2.5}$ and other atmospheric particulate matter by plant leaves: Taking *Populus tomentosa* as an example. *Chin. J. Appl. Ecol.* **2014**, *25*, 2238–2242.

35. Song, Y.S.; Maher, B.A.; Li, F.; Wang, X.K.; Sun, X. Particulate matter deposited on leaf of five evergreen species in Beijing, China: Source identification and size distribution. *Atmos. Environ.* **2015**, *105*, 53–60. [CrossRef]

36. Yan, J.; Lin, L.; Zhou, W.; Ma, K.; Pickett, S.T.A. A novel approach for quantifying particulate matter distribution on leaf surface by combining SEM and object-based image analysis. *Remote Sens. Environ.* **2016**, *173*, 156–161. [CrossRef]

37. Leonard, R.J.; McArthur, C.; Hochuli, D.F. Particulate matter deposition on roadside plants and the importance of leaf trait combinations. *Urban For. Urban Green.* **2016**, *20*, 249–253. [CrossRef]

38. Liu, J.; Cao, Z.; Zou, S.; Liu, H.; Hai, X.; Wang, S.; Duan, J.; Xi, B.; Yan, G.; Zhang, S.; et al. An investigation of the leaf retention capacity, efficiency and mechanism for atmospheric particulate matter of five greening tree species in Beijing, China. *Sci. Total Environ.* **2018**, *616–617*, 417–426. [CrossRef]

39. Xu, Y.; Xu, W.; Mo, L.; Heal, M.R.; Xu, X.; Yu, X. Quantifying particulate matter accumulated on leaves by 17 species of urban trees in Beijing, China. *Environ. Sci. Pollut. Res.* **2018**, *25*, 12545–12556. [CrossRef]

40. Hagler, G.S.W.; Lin, M.Y.; Khlystov, A.; Baldauf, R.W.; Isakov, V.; Faircloth, J.; Jackson, L.E. Field investigation of roadside vegetative and structural barrier impact on near-road ultrafine particle concentrations under a variety of wind conditions. *Sci. Total Environ.* **2012**, *419*, 7–15. [CrossRef]

41. Tong, Z.; Whitlow, T.H.; MacRae, P.F.; Landers, A.J.; Harada, Y. Quantifying the effect of vegetation on near-road air quality using brief campaigns. *Environ. Pollut.* **2015**, *201*, 141–149. [CrossRef] [PubMed]

42. Lu, S.; Yang, X.; Li, S.; Chen, B.; Jiang, Y.; Wang, D.; Xu, L. Effects of plant leaf surface and different pollution levels on $PM_{2.5}$ adsorption capacity. *Urban For. Urban Green.* **2018**, *34*, 64–70. [CrossRef]

43. Sæbø, A.; Popek, R.; Nawrot, B.; Hanslin, H.M.; Gawronska, H.; Gawronski, S.W. Plant species differences in particulate matter accumulation on leaf surfaces. *Sci. Total Environ.* **2012**, *427–428*, 347–354. [CrossRef] [PubMed]

44. Liu, L.; Guan, D.; Peart, M.R.; Wang, G.; Zhang, H.; Li, Z. The dust retention capacities of urban vegetation-a case study of Guangzhou, South China. *Environ. Sci. Pollut. Res.* **2013**, *20*, 6601–6610. [CrossRef] [PubMed]

45. Liu, J.; Zhu, L.; Wang, H.; Yang, Y.; Liu, J.; Qiu, D.; Ma, W.; Zhang, Z.; Liu, J. Dry deposition of particulate matter at an urban forest, wetland and lake surface in Beijing. *Atmos. Environ.* **2016**, *125*, 178–187. [CrossRef]

46. Giardina, M.; Buffa, P. A new approach for modeling dry deposition velocity of particles. *Atmos. Environ.* **2018**, *180*, 11–22. [CrossRef]

47. Buccolieri, R.; Gromke, C.; Sabatino, S.D.; Ruck, B. Aerodynamic effects of trees on pollutant concentrationin street canyons. *Sci. Total Environ.* **2009**, *407*, 5247–5256. [CrossRef]

48. Buccolieri, R.; Salim, S.M.; Leo, L.S.; Sabatino, S.D.; Chan, A.; Ielpo, P.; Gennaro, G.; Gromke, C. Analysis oflocal scale tree-atmosphere interaction on pollutant concentration in idealized street canyons and application to a real urban junction. *Atmos. Environ.* **2011**, *45*, 1702–1713. [CrossRef]

49. Pugh, T.A.; Mackenzie, A.R.; Whyatt, J.D.; Hewitt, C.N. Effectiveness of green infrastructure for improvement of air quality in urban street canyons. *Environ. Sci. Technol.* **2012**, *46*, 7692–7699. [CrossRef]

50. Wania, A.; Bruse, M.; Blond, N.; Weber, C. Analysing the influence of different street vegetation on traffic-induced particle dispersion using microscale simulations. *J. Environ. Manag.* **2012**, *94*, 91–101. [CrossRef] [PubMed]

51. Gromke, C.; Blocken, B. Influence of avenue-trees on air quality at the urban neighborhood scale. Part I: Quality assurance studies and turbulent Schmidt number analysis for RANS CFD simulations. *Environ. Pollut.* **2015**, *196*, 214–223. [CrossRef] [PubMed]

52. Jeanjean, A.P.R.; Monks, P.S.; Leigh, R.J. Modelling the effectiveness of urban trees and grass on PM$_{2.5}$ reduction via dispersion and deposition at a city scale. *Atmos. Environ.* **2016**, *147*, 1–10. [CrossRef]

53. Hofman, J.; Bartholomeus, H.; Janssen, S.; Calders, K.; Wuyts, K.; Van Wittenberghe, S.; Samson, R. Influence of tree crown characteristics on the local PM$_{10}$ distributioninside an urban street canyon in Antwerp (Belgium): A model and experimental approach. *Urban For. Urban Green.* **2016**, *20*, 265–276. [CrossRef]

54. Tong, Z.; Baldauf, R.W.; Isakov, V.; Deshmukhd, P.; Zhang, K.M. Roadside vegetation barrier designs to mitigate near-road air pollution impacts. *Sci. Total Environ.* **2016**, *541*, 920–927. [CrossRef]

55. Hong, B.; Lin, B.; Qin, H. Numerical investigation on the coupled effects of building-tree arrangements on fine particulate matter (PM$_{2.5}$) dispersion in housing blocks. *Sustain. Cities Soc.* **2017**, *34*, 358–370. [CrossRef]

56. Buccolieri, R.; Santiago, J.; Rivas, E.; Sanchez, B. Review on urban tree modelling in CFD simulations: Aerodynamic, deposition and thermal effects. *Urban For. Urban Green.* **2018**, *31*, 212–220. [CrossRef]

57. Tong, Z.; Chen, Y.; Malkaw, A.; Adamkiewicz, G.; Spengler, J.D. Quantifying the impact of traffic-related air pollution on the indoor air quality of a naturally ventilated building. *Environ. Int.* **2016**, *89–90*, 138–146. [CrossRef]

58. Hong, B.; Qin, H.; Jiang, R.; Xu, M.; Niu, J. How outdoor trees affect indoor particulate matter dispersion: CFD simulations in a naturally ventilated auditorium. *Int. J. Environ. Res. Public Health* **2018**, *15*, 2862. [CrossRef]

59. Qin, H.; Hong, B.; Jiang, R. Are green walls better options than green roofs for mitigating PM$_{10}$ pollution? CFD simulations in urban street canyons. *Sustainability* **2018**, *10*, 2833. [CrossRef]

60. Tong, Z.; Whitlow, T.H.; Landers, A.; Flanner, B. A case study of air quality above an urban roof top vegetable farm. *Environ. Pollut.* **2016**, *208*, 256–260. [CrossRef]

61. Yin, S.; Shen, Z.; Zhou, P.; Zou, X.; Che, S.; Wang, W. Quantifying air pollution attenuation within urban parks: An experimental approach in Shanghai, China. *Environ. Pollut.* **2011**, *159*, 2155–2163. [CrossRef]

62. Paoletti, E.; Bardelli, T.; Giovannini, G.; Pecchioli, L. Air quality impact of an urban park over time. *Procedia Environ. Sci.* **2011**, *4*, 10–16. [CrossRef]

63. Lam, K.C.; Ng, S.L.; Hui, W.C.; Chan, P.K. Environmental quality of urban parks and open spaces in Hong Kong. *Environ. Monit. Assess.* **2005**, *111*, 55–73. [CrossRef] [PubMed]

64. Jim, C.Y.; Chen, W.Y. Assessing the ecosystem service of air pollutant removal by urban trees in Guangzhou (China). *J. Environ. Manag.* **2008**, *88*, 665–676. [CrossRef] [PubMed]

65. Holmes, N.S.; Morawska, L. A review of dispersion modeling and its application to the dispersion of particles: An overview of different dispersion models available. *Atmos. Environ.* **2006**, *40*, 5902–5928. [CrossRef]

66. Yang, A.S.; Juan, Y.H.; Wen, C.Y.; Chang, C.J. Numerical simulation of cooling effect of vegetation enhancement in a subtropical urban park. *Appl. Energy* **2017**, *192*, 178–200. [CrossRef]

67. Xue, F.; Li, X. The impact of roadside trees on traffic released PM$_{10}$ in urban street canyon: Aerodynamic and deposition effects. *Sustain. Cities Soc.* **2017**, *30*, 195–204. [CrossRef]

68. Barratt, R. *Atmospheric Dispersion Modeling: An Introduction to Practical Applications*; Earthscan Publications: London, UK, 2001.

69. Shaanxi Meteorological Bureau. Real-Time Air Quality in Xi'an. Available online: www.sxmb.gov.cn (accessed on 13 January 2018).

70. Bruse, M.; Fleer, H. Simulating surface–plant–air interactions inside urban environments with a three dimensional numerical model. *Environ. Model. Softw.* **1998**, *13*, 373–384. [CrossRef]

71. Srivanit, M.; Hokao, K. Evaluating the cooling effects of greening for improving the outdoor thermal environment at an institutional campus in the summer. *Build. Environ.* **2013**, *66*, 158–172. [CrossRef]

72. Liu, J.; Zhai, J.; Zhu, L.; Yang, Y.; Liu, J.; Zhang, Z. Particle removal by vegetation: comparison in a forest and a wetland. *Environ. Sci. Pollut. R.* **2017**, *24*, 1597–1607. [CrossRef]

73. Franke, J.; Hellsten, A.; Schlunzen, K.H.; Carissimo, B. The COST 732 best practice guideline for CFD simulation of flows in the urban environment: A summary. *Int. J. Environ. Pollut.* **2011**, *44*, 419–427. [CrossRef]

74. Lin, B.; Li, X.; Zhu, Y.; Qin, Y. Numerical simulation studies of the different vegetation patterns' effect on outdoor pedestrian thermal comfort. *J. Wind Eng. Ind. Aerod.* **2008**, *96*, 1707–1718. [CrossRef]

75. Sanz, C. A note on k-epsilon modelling of vegetation canopy air-flows. *Bound.-Layer Meteorol.* **2003**, *108*, 191–197. [CrossRef]

76. Katul, G.G.; Mahrt, L.; Poggi, D.; Sanz, C. One- and two-equation models for canopy turbulence. *Bound.-Layer Meteorol.* **2004**, *113*, 81–109. [CrossRef]

77. Endalew, A.M.; Hertog, M.; Delele, M.A.; Baetens, K.; Persoons, T.; Baelmans, M.; Ramon, H.; Nicolai, B.M.; Verboven, P. CFD modelling and wind tunnel validation of airflow through plant canopies using 3D canopy architecture. *Int. J. Heat Fluid Flow* **2009**, *30*, 356–368. [CrossRef]

78. Zhao, B.; Chen, C.; Tan, Z. Modeling of ultrafine particle dispersion in indoor environments with an improved drift flux model. *J. Aerosol Sci.* **2009**, *40*, 29–43. [CrossRef]

79. Nowak, D.J.; Hirabayashi, S.; Bodine, A.; Hoehn, R. Modeled $PM_{2.5}$ removal by trees in ten U.S. cities and associated health effects. *Environ. Pollut.* **2013**, *178*, 395–402. [CrossRef]

80. Ministry of Urban and Rural Construction of the People's Republic of China. *Standard for Design of Urban Park (CJJ 48-92)*; China Architecture & Building Press: Beijing, China, 1992. (In Chinese)

81. Roache, P.J. Perspective: A method for uniform reporting of grid refinement studies. *J. Fluids Eng.* **1994**, *116*, 405–413. [CrossRef]

82. Hefny, M.M.; Ooka, R. CFD analysis of pollutant dispersion around buildings: Effect of cell geometry. *Build. Environ.* **2009**, *44*, 1699–1706. [CrossRef]

83. Gromke, C.; Buccolieri, R.; Di Sabatino, S.; Ruck, B. Dispersion study in a street canyon with tree planting by means of wind tunnel and numerical investigations—Evaluation of CFD data with experimental data. *Atmos. Environ.* **2008**, *42*, 8640–8650. [CrossRef]

84. Neft, I.; Scungio, M.; Culver, N.; Singh, S. Simulations of aerosol filtration by vegetation: Validation of existing models with available lab data and application to near-roadway scenario. *Aerosol Sci. Technol.* **2016**, *50*, 937–946. [CrossRef]

85. Mitchell, R.; Maher, B.A.; Kinnersley, R. Rates of particulate pollution deposition onto leaf surfaces: Temporal and inter-species magnetic analyses. *Environ. Pollut.* **2010**, *158*, 1472–1478. [CrossRef]

86. Jin, S.; Guo, J.; Wheeler, S.; Kan, L.; Che, S. Evaluation of impacts of trees on $PM_{2.5}$ dispersion in urban streets. *Atmos. Environ.* **2014**, *99*, 277–287. [CrossRef]

87. Salmond, J.A.; Williams, D.E.; Laing, G.; Kingham, S.; Dirks, K.; Longley, I.; Henshaw, G.S. The influence of vegetation on the horizontal and vertical distribution of pollutants in a street canyon. *Sci. Total Environ.* **2013**, *443*, 287–298. [CrossRef] [PubMed]

88. Jeanjean, A.P.R.; Buccolieri, R.; Eddy, J.; Monks, P.S.; Leigh, R.J. Air quality affected by trees in real street canyons: The case of Marylebone neighbourhood in central London. *Urban For. Urban Green.* **2017**, *22*, 41–53. [CrossRef]

89. WHO. *Air Quality Guidelines for Particulate Matter, Ozone, Nitrogen Dioxide and Sulfur Dioxide*; WHO: Geneva, Switzerland, 2005.

90. Wu, H.; Yang, C.; Chen, J.; Yang, S.; Lu, T.; Lin, X. Effects of green space landscape patterns on particulate matter in Zhejiang province, China. *Atmos. Pollut. Res.* **2018**, *9*, 923–933. [CrossRef]

91. Chen, C.; Zhao, B. Review of relationship between indoor and outdoor particles: I/O ratio, infiltration factor and penetration factor. *Atmos. Environ.* **2011**, *45*, 275–288. [CrossRef]

92. Chithra, V.S.; Shiva Nagendra, S.M. Impact of outdoor meteorology on indoor PM_{10}, $PM_{2.5}$ and PM_1 concentrations in a naturally ventilated classroom. *Urban Clim.* **2014**, *10*, 77–91. [CrossRef]

93. Mohammadyan, M.; Ghoochani, M.; Kloog, I.; Abdul-Wahab, S.A.; Yetilmezsoy, K.; Heibati, B.; Pollitt, K.J.G. Assessment of indoor and outdoor particulate air pollution at an urban background site in Iran. *Environ. Monit. Assess.* **2017**, *189*, 235. [CrossRef]